# Self-Balancing Exoskeleton Robots Designed to Facilitate Multiple Rehabilitation Training Movements

Dingkui Tian, Wentao Li, Jinke Li, Feng Li, Ziqiang Chen, Yong He, Jianquan Sun, and Xinyu Wu, *Senior Member, IEEE*

***Abstract*— This study presents the biomimetic design of the structure and controller of AutoLEE-II, a self-balancing exoskeleton developed to assist patients in performing multiple rehabilitation movements without crutches or other supporting equipment. Its structural design is founded upon the human body structure, with an eliminated axis deviation and a raised CoM of the exoskeleton. The controller is a physical parameter-independent controller based on the CoM modification. Thus, the exoskeleton can adapt to patients with different physical parameters. Five subjects underwent exoskeleton-assisted rehabilitation training experiments, including squatting, tilting, and walking trainings. The results showed that the exoskeleton can assist patients in completing various rehabilitation exercises and help them maintain their balance during the rehabilitation training. This helpful role of the exoskeleton in rehabilitation training is analyzed through an electromyography (EMG) data analysis. The findings revealed that wearing the exoskeleton can reduce the activity of the lower limb muscles by approximately 20–30% when performing the same rehabilitation exercises.**

***Index Terms*— Rehabilitation, self-balancing exoskeleton, biomimetic structure, physical parameter-independent controller.**

Manuscript received 15 August 2023; revised 7 December 2023; accepted 26 December 2023. Date of publication 1 January 2024; date of current version 16 January 2024. The work of Xinyu Wu was supported in part by the National Natural Science Foundation of China under Grant 62125307 and Grant 62373346, in part by the Shenzhen Basic Research Project JCYJ20220818101416035, and in part by the NSFC-Shenzhen Robotics Research Center Project U2013207 and Project U2013209. *(Corresponding author: Xinyu Wu.)*

This work involved human subjects or animals in its research. Approval of all ethical and experimental procedures and protocols was granted by the Medical Ethics Committee of Shenzhen Institute of Advanced Technology under Application No. SIAT-IRB-200715-H0512.

Dingkui Tian, Wentao Li, Jinke Li, Ziqiang Chen, Jianquan Sun, and Xinyu Wu are with the Guangdong Provincial Key Laboratory of Robotics and Intelligent System, Shenzhen Institute of Advanced Technology, Chinese Academy of Sciences, Shenzhen 518055, China, and also with the SIAT CUHK Joint Laboratory of Robotics and Intelligent Systems, Shenzhen 518055, China (e-mail: dk.tian1@siat.ac.cn; wt.li@siat.ac.cn; jk.li@siat.ac.cn; zq.chen1@siat.ac.cn; jq.sun@siat.ac.cn; xy.wu@siat.ac.cn).

Feng Li is with the Guangdong Provincial Key Laboratory of Robotics and Intelligent System, Shenzhen Institute of Advanced Technology, Chinese Academy of Sciences, Shenzhen 518055, China, also with the SIAT CUHK Joint Laboratory of Robotics and Intelligent Systems, Shenzhen 518055, China, and also with the Shenzhen College of Advanced Technology, University of Chinese Academy of Sciences, Shenzhen 518055, China (e-mail: feng.li@siat.ac.cn).

Yong He is with the Guangdong Provincial Key Laboratory of Robotics and Intelligent System, Shenzhen Institute of Advanced Technology, Chinese Academy of Sciences, Shenzhen 518055, China, also with the SIAT CUHK Joint Laboratory of Robotics and Intelligent Systems, Shenzhen 518055, China, and also with China Construction Third Bureau First Engineering MEP Company Ltd., Shenzhen 518109, China (e-mail: mr.yonghe@hotmail.com).

Digital Object Identifier 10.1109/TNSRE.2023.3348985

## I. Introduction

SPINAL cord injury (SCI) is a multifaceted disease that can lead to a range of disabilities, including partial or complete loss of one's locomotion function. Individuals with SCI are highly vulnerable to various secondary health conditions (SHCs) [1], [2]. To restore mobility, prevent SHCs, and improve a patient's quality of life, physical therapy and rehabilitation training are widely used in SCI treatments [3]. Lower limb exoskeletons have been proven to effectively assist individuals undergoing rehabilitation training and SCI treatments. Several exoskeletons, such as ReWalk [4], Ekso [5], HAL [6], and Indego [7], have successfully been validated for various clinical applications. However, most exoskeletons do not have a self-balance ability; hence, individuals with SCI are required to use additional support devices (e.g., crutches) to maintain balance during rehabilitation training. In other words, these exoskeletons are primarily suitable for SCI individuals with an able upper limb. Even for SCI individuals with strong upper limbs, the long-term use of support devices during exoskeleton-assisted rehabilitation training poses the risk of shoulder joint injuries. Therefore, it is essential to design an exoskeleton that can provide self-balance and perform various rehabilitation movements. This, however, presents significant difficulties in both structural and control algorithm designs.

### A. Structure Design of the Lower Limb Exoskeleton

In terms of the structure design, many lower limb exoskeletons with an innovative structure have been explored to assist SCI individuals in rehabilitation training and walking assistive service. The Indego exoskeleton has four actuated joints because it is specifically designed to assist in the movement of an individual's hip and knee joints in the sagittal plane [8]. The Mindwalker exoskeleton with 10 degrees of freedom (DOFs)

has six actuated joints that add active hip abduction/adduction joints for weight shift and lateral foot placement. It can provide gait assistance in both the sagittal and frontal planes [9]. Meanwhile, the Symbitron exoskeleton has eight powered joints and four passive joints, among which actuated joints add ankle dorsi/plantarflexion. Therefore, Symbitron can achieve a more stable sagittal plane walking performance [10]. However, the numbers of the actuated joints of the abovementioned exoskeletons are not enough to provide rehabilitation training and walking assistance to all the lower limb joints of SCI individuals in the self-balance mode.

The REX exoskeleton developed by REX Bionics (New Zealand) is a self-balance exoskeleton with 10 actuated joints. It features two hip joints, one knee joint, and two ankle joints that facilitate movement in the sagittal and lateral planes. However, it cannot perform turning movements because it lacks hip endo/exorotation joints [11]. Atalante, which is a self-balancing lower limb exoskeleton developed and produced by the French company, Wandercraft, is fitted with 12 powered joints that allow for movement in the sagittal, frontal, and transverse planes. It can effectively assist all the lower limb joints of an SCI individual during self-balancing rehabilitation training and walking assistive services [12]. Wu et al. designed and developed a novel self-balancing exoskeleton, called AutoLEE-I. Its structure with 10 actuated DOFs is similar to that of REX. AutoLEE-I cannot assist in rehabilitation training on turning movements because it does not have hip endo/exorotation acutated joints [13]. Self-balancing lower limb exoskeletons are designed to fulfill only the fundamental functional requirements necessary for rehabilitation training and walking assistance services for the partial lower limb joints of SCI individuals in the self-balancing mode. They do not undergo structural optimization based on biomimetic principles, leading to insufficient stiffness and axis deviation. The lack of structure stiffness increases the difficulty of controlling exoskeletons, while axis deviation, especially in the hip joints, causes significant user discomfort.

### B. Control of Rehabilitation Training and Walking Assistance

Dzeladini et al. proposed a neuromuscular controller (NMC) that generates motion in accordance with both the user's abilities and natural walking dynamics. Based on a neuromuscular model, the NMC generates the corresponding joint trajectories with a few sensory input, instead of directly using the libraries of the desired joint trajectories. This ensures compliance for patients with a remaining function [14], [15], [16]. The proportional myoelectric controller relies on direct EMG control schemes. It directly generates the required torque for joints by measuring the electromyogram signals obtained from the human body. Despite their advantages, the aforementioned control strategies only ensure that the generated gait trajectories can closely simulate the human gait, without considering the walking stability. Hence, they cannot perform rehabilitation training and walking assistive services during the self-balancing mode.

Some controllers achieve the self-balancing locomotion for the exoskeleton. REX Bionics utilized Euler equations and applied the theory of the CoM dynamics to develop a CoM compensation approach that stabilizes their exoskeleton during walking [6]. However, the control strategy of REX does not incorporate compliant elements. This results in significant impact forces between the exoskeleton and the ground, which leads to a poor stability. Li proposed a novel human-in-the-loop controller that divides the task workspaces into human-voluntary and robot-constrained regions. The controller constrains the user's lower limb motion to a compliant region around various desired trajectories. As a result, flat walking, turning, and crossing the obstacle were realized [17]. Atalante is a 12 DOFs actuated self-balancing exoskeleton designed by Wandercraft. Wandercraft developed a mathematical hybrid dynamics model and applied the hybrid zero dynamicsthe hybrid zero dynamics (HZD) control method to achieve self-balance walking on flat ground [18], [19], [20]. The human-in-the-loop and HZD controllers were based on an accurate mathematical model of both the exoskeleton and the user [6]. However, getting precise parameters for the human-exoskeleton dynamics can be difficult. Moreover, the changes in individual users can alter the physical dynamics. Consequently, the human-in-the-loop and HZD controllers are not suitable for exoskeletons with variable wearers.

### C. Study Contribution

We aimed herein to develop a self-balancing exoskeleton capable of facilitating multiple rehabilitation movements, to ensure that individuals with varying conditions can complete rehabilitation training with the exoskeleton's help. As regards its structural design, an adequate biomimetic design is necessary for the exoskeleton structure to correspond with the joints of human's lower limb and perform various rehabilitation movements. The structure must be compatible with the human body for it to be able to provide appropriate assistance while worn. The self-balancing walking control algorithms of the exoskeleton require sufficient robustness to physical parameters to adapt to various wearers. To satisfy the mentioned requirements, a self-balancing exoskeleton, called AutoLEE-II, which has 12 actuated DOFs, was developed. In this work, we will introduce the structural and control algorithm designs of AutoLEE-II. AutoLEE-II achieves self-balancing walking and enables several rehabilitation movements, including squatting, tilting, and walking, through a CoM modification controller based on the centroid dynamics. We will conduct experiments on exoskeleton-assisted rehabilitation training and analyze the exoskeleton's ability to facilitate different rehabilitation movements, maintain balance, and aid SCI individuals during the rehabilitation process. The main contributions of this work are as follows:

- AutoLEE-II, a self-balancing exoskeleton with 12 DOFs, is designed. Its structure features a high degree of biomimicry and compatibility with the human body.
- A CoM modification controller based on the centroid dynamics is proposed to ensure the self-balancing ability of AutoLEE-II. To adapt to different wearers, the controller is made to have sufficient robustness to physical parameters.

- Multiple exoskeleton -assisted balance and gait rehabilitation experiments are designed. The raining effects of different subjects wearing AutoLEE-II are demonstrated through the EMG analysis.

The remainder of this paper is organized as follows. Section II introduces the structure design and the controller of AutoLEE-II; Section III discusses the exoskeleton-assisted rehabilitation training experiment and relevant analysis; and Section IV provides the conclusions.

## II. Self-Balancing Lower Limb Exoskeleton System

The exoskeleton structure must be designed in a biomimetic manner to provide proper assistance to the patient's lower limb joints during the rehabilitation training, which involves different movements, and achieve compatibility between the human body and the exoskeleton. To do this, we first analyzed the human anatomy and obtained the joint distribution of AutoLEE-II based on this. We then designed a series-parallel hybrid joint mechanism to eliminate the axis deviation and improve the structural stiffness.

The human hip is a 3-DOF ball-and-socket joint capable of hip adduction/abduction (HAA), hip flexion/extension (HFE), and hip endo/exorotation (HEE). The human knee is a 1-DOF hinge joint that allows for knee flexion/extension (KFE). The human ankle is a 3-DOF saddle joint comprising ankle inversion/eversion (AIE), ankle dorsi/plantarflexion (ADP), and ankle endo/exorotation (AEE). Anthropotomy divides human movements into three motion planes: sagittal, frontal, and transverse planes. The three basic rotation axes are the sagittal, coronal, and vertical axes. Due to the rotational movements of the hip–knee–ankle joints in the sagittal plane providing the main power for the human locomotion, the HFE, KFE, and ADP actuators are essential for providing power for the human locomotion [8]. The HAA and ADP actuators are the keys to the weight shift and lateral foot placement that assists in maintaining balance [9]. The AIE actuator is crucial for maintaining balance. The rotational movements of the ankle joint in the coronal plane provide major assistance for maintaining balance, especially when the exoskeleton performs lateral tilting movements. Therefore, the most basic requirement for achieving self-balancing assistance without external support is to power the flexion/extension and the abduction/adduction rotation of the hip, knee, and ankle joints in the sagittal plane, as well as the external/internal rotation of the hip and ankle joints in the coronal plane. Considering that the HEE actuator is the basis for the exoskeleton to perform more rehabilitation actions (e.g., turning while walking,), the exoskeleton was determined to have 12 actuated joints, as shown in Fig. 1.

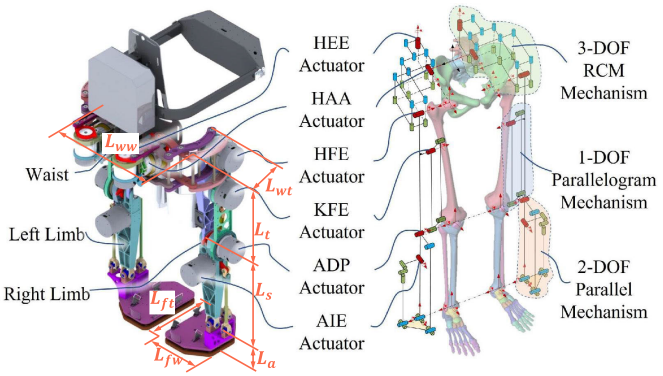


Fig. 1. Biomimetic mechanism design of AutoLEE-II. The joint distribution is based on the human anatomy. The structure has high compatibility with the human body. The various dimensional features of the exoskeleton are depicted by the orange lines in the figure.

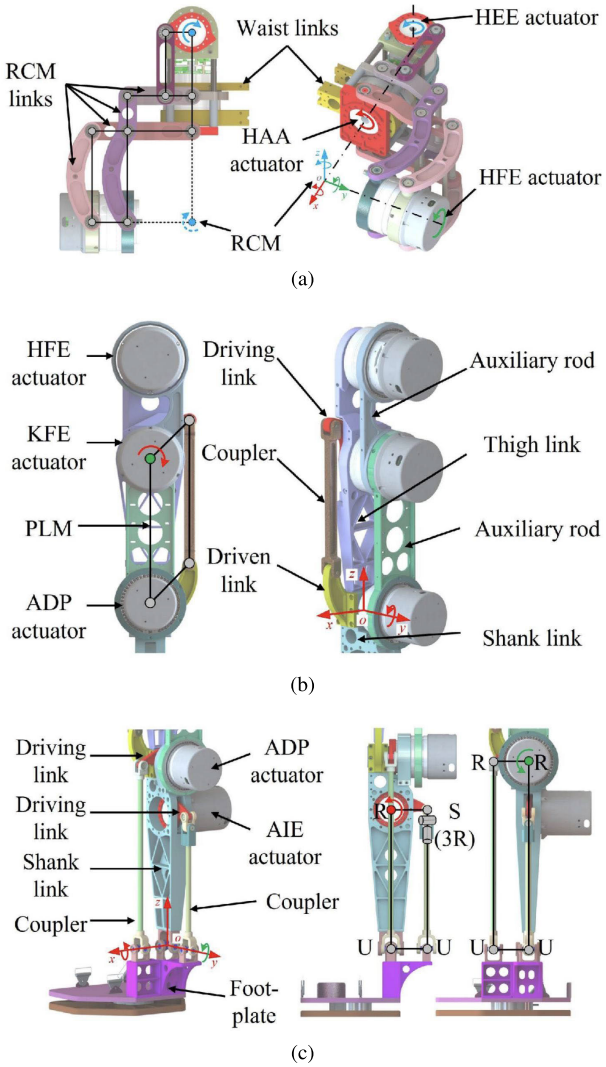


Fig. 2. Mechanical structure of each exoskeleton joint. A series–parallel hybrid mechanism is designed to increase the structural stiffness and reduce the leg's moment of inertia. (a) Hip joint structure. (b) Knee joint structure. (c) Ankle joint structure.

### A. Biomimetic Structural Design

The mechanical structures of the hip, knee, and ankle joints are crucial for improving the exoskeleton's compatibility with the human body. This is especially important when designing the exoskeleton hip joint. As shown in Fig. 2a, the hip joint of AutoLEE-II was designed with 3 DOFs: HAA, HEE, and HFE. We designed a series–parallel hybrid mechanism for the hip joint based on the remote center of motion (RCM) mechanism to improve the kinematic compatibility between the human body and the exoskeleton. With this design, the

TABLE I
LINK LENGTH OF AUTOLEE-II

| Link parameters | $L_t$ | $L_s$ | $L_a$ | $L_{wt}$ | $L_{ww}$ | $L_{fw}$ | $L_{ft}$ |
|---|---|---|---|---|---|---|---|
| Values/mm | 440 | 400 | 136 | 200 | 400 | 130 | 290 |

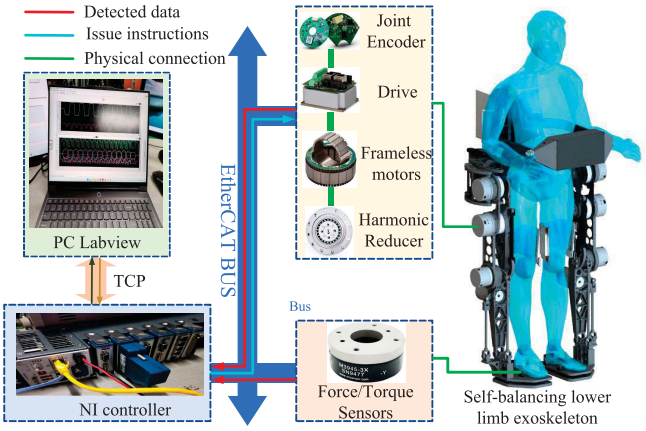


Fig. 3. Control and communication system of the exoskeleton.

rotation axes of the HAA, HEE, and HFE intersect at the center of the human hip joint, consequently eliminating the motion axis misalignment. The upper and lower double-layer RCM links are connected in parallel to improve the structural stiffness of the exoskeleton hip joint. The HAA and HFE actuators are located between the RCM connecting rods as shown in Fig. 2a. The structural designs of the knee joint with 1 DOF and the ankle joint with 2 DOFs are simpler. The KFE actuator is designed to connect the thigh link to the shank link and provide 1 DOF for knee flexion and extension, as described in Fig. 2b. A novel parallel mechanism with 2 DOFs is utilized to produce the inversion/eversion and dorsi/plantarflexion motions of the exoskeleton ankle joint. The KFE actuator is mounted on the thigh link as close to the HFE actuator as possible to improve the CoM position of the exoskeleton (shown in Fig. 2c). More details of the structure design of AutoLEE-II can be found in [21].

AutoLEE-II mainly aims to provide rehabilitation training and locomotion assistance for patients with SCI. Thus, it is equipped with several straps that serve as connectors between the person and the device. Two of these straps are attached to the thigh to connect the human thigh to the exoskeleton. The other two straps can be found at the foot to connect the foot and the exoskeleton. The exoskeleton height is approximately 1.6 m. Its total weight is 84.7 kg. The lengths of the AutoLEE-II links are obtained from the anthropometric data of the body height between 150 and 185 cm. $L_t$, $L_s$, $L_a$, $L_{wt}$, $L_{ww}$, $L_{ft}$, and $L_{fw}$ represent the thigh link length, shank link length, distance from the ankle joint center to the ground, exoskeleton waist thickness, exoskeleton waist width, foot thickness, and foot width respectively as shown in Fig. 1. Table II lists each variable value.

### B. Control Architecture

Fig. 3 depicts the control and communication system. National Instruments (NI) controller is the exoskeleton's control center. For each joint, Elmo drivers are utilized to exchange the control command with the NI controller, while absolute encoders are used to determine the absolute position. Force/torque (F/T) sensors are placed at the middle position between the upper and lower footplates to measure the zero moment point (ZMP).

The communication between the NI controller and the PC is achieved via the TCP protocol. To ensure the controller's real-time performance, the communication among the NI controller, F/T sensors, and Elmo drivers is achieved via a bus based on the Ethernet for Control Automation Technologe protocol. A 0.25–1 kHz control frequency of the close loop can easily be achieved with this control structure. The control frequency of the close loop in this work is 1 kHz.

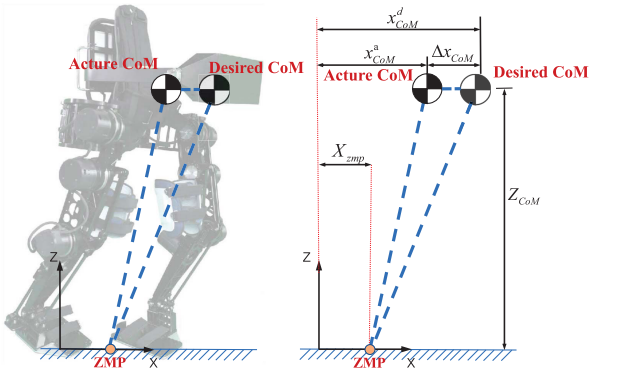


Fig. 4. AutoLEE-II and its simplified linear inverted pendulum model (LIPM). The deviation between the actual and desired CoM is calculated using the CoM modification controller.

## III. CONTROL FRAMEWORK

The linear inverted pendulum model (LIPM) is a reliable simplified physical model for exoskeleton robots [22]. The dynamic equation of the LIPM is independent of mass, making it robust to wearers with different physical parameters. We simplified AutoLEE-II as the LIPM as shown in Fig. 4. The LIPM motion in the sagittal plane was independent of the motion in the frontal plane, and the form was consistent [23]. We will only derive the equations in the sagittal plane. in the subsequent section.

The control framework was divided into three parts: gait generator, inverse kinematics solver, and CoM modification controller as shown in Fig. 5. The gait generator generated the foot reference positions and the reference ZMP trajectories based on the predetermined motion parameters (e.g., movement actions and step length) and obtained the reference trajectory of the CoM through the centroid dynamics of the LIPM. The inverse kinematics solver determined the joint angle based on the foot reference and CoM trajectories. The CoM modification controller calculated the CoM modification based on the error between the reference and actual ZMPs obtained from the F/T sensors. The contents are explained in detail below.

### A. Gait Generator

The gait generator generated the foot and ZMP positions based on the predetermined motion parameters. We designed

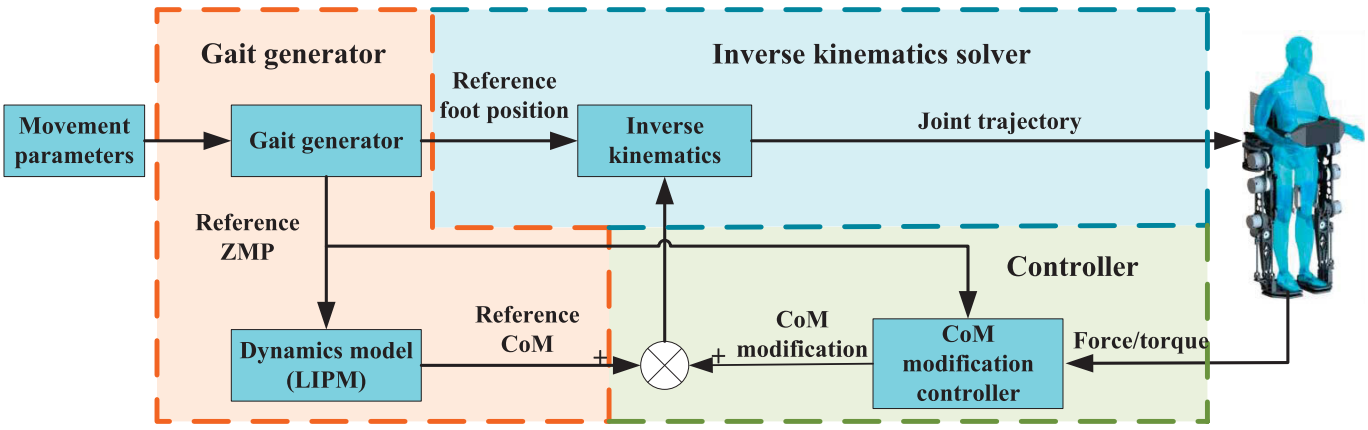


Fig. 5. The feedback controller based on the ZMP of AutoLEE-II. The controller consists of three parts, namely: gait generator, inverse kinematics calculator, and feedback controller.

a preview control based on the LIPM designed to generate the CoM trajectory that satisfies the LIPM dynamic equation [24], [25]. The positions of the feet and the CoM trajectory can be used to obtain the angles of each exoskeleton joint.

### B. Inverse Kinematics Solver

The inverse kinematics solver was designed for calculating the angles of each joint using the positions of the feet and the CoM. The rotation axes of the three DOFs of the hip joint intersect at one point; hence, a closed-form solution for the inverse kinematics model exists. In our previous work, a geometric method-based solution was developed to solve the inverse kinematics problem of AutoLEE-II [21].

### C. CoM Modification Controller

The exoskeleton may experience premature contact with the ground during locomotion. An imbalance is then caused by the impact. This phenomenon manifests in a significant discrepancy between the actual and reference ZMPs in the sensor data. The CoM modification controller aims to improve the ZMP tracking accuracy and enhance the exoskeleton's self-balancing performance by compensating for the CoM position.

The LIPM in the sagittal plane is expressed as follows:

$$m(\ddot{z}_{CoM}+g)(x_{CoM}-x_{zmp})-m(z_{CoM}-z_{zmp})\ddot{x}_{CoM}=0 \tag{1}$$

where $[x_{CoM}, z_{CoM}]^T$, $[x_{zmp}, y_{zmp}]^T$, $m$, and $g$ denote the CoM position, ZMP position, exoskeleton robot's mass, and gravity acceleration, respectively.

We assumed that the ground is flat, and the exoskeleton does not tip over. In other words, the CoM height in the z-direction is constant. Walking in this condition is expressed as follows:

$$z_{CoM}=z_c,\ \ddot{z}_{CoM}=0,\ z_{zmp}=0 \tag{2}$$

Integrating Eq. (2) into Eq. (1) yields the following dynamics of AutoLEE-II walking on a flat ground:

$$x_{zmp}=x_{CoM}-\frac{z_{CoM}}{g}\ddot{x}_{CoM} \tag{3}$$

The dynamic equation of the LIPM is independent of the physical parameters of AutoLEE-II and the wearer, meaning that the changes in the exoskeleton mass will not affect the controller stability. In short, AutoLEE-II can adapt to various wearers.

The actual ZMP was calculated from the data measured by the F/T sensors with reference to the method proposed by [26]. A fixed controlled time delay $T$ exists between the real and detected ZMPs, which, in complex domain, can be expressed as follows:

$$x_{zmp}=\frac{1}{Ts+1}\hat{x}_{zmp} \tag{4}$$

where $x_{zmp}$ is the real ZMP, and $\hat{x}_{zmp}$ is the detected ZMP. The delay time of the ZMP in this work is $T$=0.001s, similar to the control time of AutoLEE-II. Substituting Eq. (4) into the centroid dynamics equation (3) yields

$$T\dot{x}_{zmp}+x_{zmp}=x_{CoM}-\frac{z_{CoM}}{g}\ddot{x}_{CoM} \tag{5}$$

The state equation is established as follows according to Eq. (5):

$$\begin{cases}\dfrac{d}{dt}\begin{bmatrix}x_{zmp}\\x_{CoM}\\\dot{x}_{CoM}\end{bmatrix}=\begin{bmatrix}-\frac{1}{T}&\frac{1}{T}&0\\0&0&1\\0&0&0\end{bmatrix}\begin{bmatrix}x_{zmp}\\x_{CoM}\\\dot{x}_{CoM}\end{bmatrix}+\begin{bmatrix}-\frac{z_{CoM}}{gT}\\0\\1\end{bmatrix}\ddot{x}_{CoM}\\ x_{zmp}=\begin{bmatrix}1&0&0\end{bmatrix}\begin{bmatrix}x_{zmp}\\x\\\dot{x}\end{bmatrix}\end{cases} \tag{6}$$

The state equation is rewritten as follows according to Eq. (6):

$$\begin{cases}\dot{\boldsymbol{\vartheta}}_{\boldsymbol{x}}=\boldsymbol{A}_{\boldsymbol{x}}\boldsymbol{\vartheta}_{\boldsymbol{x}}+\boldsymbol{b}_{\boldsymbol{x}}u_x\\ y_x=\boldsymbol{C}_{\boldsymbol{x}}\boldsymbol{\vartheta}_{\boldsymbol{x}}\end{cases} \tag{7}$$

where $\boldsymbol{\vartheta}_{\boldsymbol{x}}=[x_{zmp}, x_{CoM}, \dot{x}_{CoM}]^T$, $u_x=\ddot{x}_{CoM}$, and $\boldsymbol{A}_{\boldsymbol{x}}=\begin{bmatrix}-\frac{1}{T}&\frac{1}{T}&0\\0&0&1\\0&0&0\end{bmatrix}$, $\boldsymbol{b}_{\boldsymbol{x}}=\begin{bmatrix}\frac{-z_{CoM}}{gT}\\0\\1\end{bmatrix}$ and $\boldsymbol{C}_{\boldsymbol{x}}=\begin{bmatrix}1&0&0\end{bmatrix}$.

The desired state equation is given as

$$\begin{cases} \dot{\boldsymbol{\vartheta}}_{\boldsymbol{x}}^{\boldsymbol{d}} = \boldsymbol{A}_{\boldsymbol{x}} \boldsymbol{\vartheta}_{\boldsymbol{x}}^{\boldsymbol{d}} + \boldsymbol{b}_{\boldsymbol{x}} \boldsymbol{u}_{\boldsymbol{x}}^{\boldsymbol{d}} \\ y_x^d = \boldsymbol{C}_{\boldsymbol{x}} \boldsymbol{\vartheta}_{\boldsymbol{x}}^{\boldsymbol{d}} \end{cases} \tag{8}$$

By subtracting the Eq. (7) from the Eq. (8), the difference between the actual and desired values is expressed as

$$\begin{cases} \boldsymbol{\Delta \dot{\vartheta}_x} = \boldsymbol{A_x \Delta \vartheta_x} + \boldsymbol{b_x \Delta u_x} \\ \Delta y_x = \boldsymbol{C_x \Delta \vartheta_x} \end{cases} \tag{9}$$

The feedback control law is given as

$$\Delta u_x = -\boldsymbol{K_\vartheta \Delta \vartheta}_x \tag{10}$$

The walking problem is written as a linear quadratic optimal control problem. The quadratic performance index is given as

$$J = \int_0^{+\infty} \left[ \boldsymbol{\Delta \vartheta}_{\boldsymbol{x}}^{\boldsymbol{T}} \left( \boldsymbol{C}_{\boldsymbol{x}}^{\boldsymbol{T}} \boldsymbol{Q}_{\boldsymbol{\vartheta}} \boldsymbol{C}_{\boldsymbol{x}} \right) \boldsymbol{\Delta \vartheta} + \Delta u_x^T \boldsymbol{R}_{\boldsymbol{\vartheta}} \Delta u_x \right] dt \tag{11}$$

where $\boldsymbol{Q}_{\boldsymbol{\vartheta}}$ is a symmetric semidefinite matrix of real numbers, and $\boldsymbol{R}_{\boldsymbol{\vartheta}}$ is a symmetric positive definite matrix of real numbers.

$K_\vartheta$ can be obtained by solving the linear quadratic optimal control problem. A more specific formulation for the feedback controller can be written as

$$\Delta \ddot{x}_{CoM} = -\boldsymbol{K_\vartheta}[1]\Delta x_{zmp} - \boldsymbol{K_\vartheta}[2]\Delta x_{CoM} - \boldsymbol{K_\vartheta}[3]\Delta \dot{x}_{CoM} \tag{12}$$

where $K_{\vartheta[i]}$ represents the $i$th element of $K_\vartheta$. The CoM $\Delta x_{CoM}$ and $\Delta \dot{x}_{CoM}$ compensation can be obtained as follows by a numerical iteration:

$$\begin{cases} \Delta \dot{x}_{CoM} = \Delta \dot{x}_{CoM} + \Delta \ddot{x}_{CoM} \cdot T \\ \Delta x_{CoM} = \Delta x_{CoM} + \Delta \dot{x}_{CoM} \cdot T \end{cases} \tag{13}$$

The compensation of COM $\Delta x_{CoM}$ is added to the desired CoM to modify the real CoM and ensure the exoskeleton balance:

$$x_{\mathrm{CoM}} = x_{\mathrm{CoM}}^d + \Delta x_{\mathrm{CoM}} \tag{14}$$

where, $x_{\mathrm{CoM}}^d$is the desired CoM.

The centroid dynamics equations in the sagittal and frontal planes are independent and have the same formulation; thus, the CoM compensation in the y axis $\Delta y_{CoM}$ can be easily derived in the same way:

$$y_{CoM} = y_{CoM}^d + \Delta y_{CoM} \tag{15}$$

where $y_{\mathrm{CoM}}^d$ is the desired CoM in the y axis. The command of angle for each joint is calculated using the modified CoM and the feet positions.

In this paper, we set $Q_\vartheta$ as 1 and $R_\vartheta$ as 0.001. Then $K_\vartheta$ can be obtained by solving the linear quadratic optimal control problem. However, given the disparity between the accurate exoskeleton model and LIPM, the parameters used in experiments require fine-tuning based on the previously obtained $K_\vartheta$, and the parameters that have been fine-tuned can be applied to various participants, without the need for further adjustments. The controller parameters $K_\vartheta$ are given in the following table:

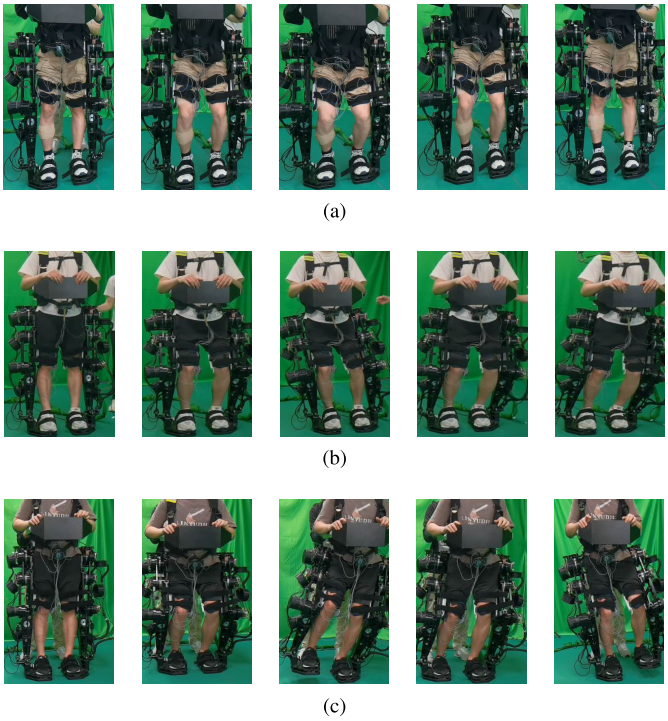

Fig. 6. Experiment snapshots: (a) Snapshots of the squatting exercise experiment. (b) Snapshots of the tilting exercise experiment. (c) Snapshots of the walking exercise experiment.

## IV. Experiments and Results

### A. Rehabilitation Training Experiment Design

Physical therapy performed by a rehabilitation therapist is generally divided into five components: range of motion (ROM) and stretching, strengthening, transfer training, balance rehabilitation training, and walking rehabilitation training [3]. In this study, the exoskeleton-assisted rehabilitation training included balance and walking rehabilitation trainings. Balance rehabilitation training was selected to increase the patient's safety with ambulation and decrease the fall risk. Multiple studies showed that balance is one of the requirements for a successful ambulation, further supporting the importance of balance rehabilitation training [27], [28], [29]. The benefits of using exoskeletons in these rehabilitation programs are an essential factor. This is especially true for the balance rehabilitation training that aims to widen the patients' limits of stability (LoS) and improve their balancing ability [30]. In the balance rehabilitation training, patients need to tilt their body and shift their CoM toward the edge of the support surface while keeping their feet still [31], [32]. For patients with a limited balancing ability, the use of exoskeletons can provide adequate external support to make the balance rehabilitation training feasible and safe. The exoskeleton enables patients to extend the range of their CoM movement, making the balance rehabilitation training more effective.

To verify the exoskeleton's balancing ability and its capability of assisting patients in their rehabilitation training, five males (25 $\pm$ 2 years old, 1.74 $\pm$ 0.05 m, 70 $\pm$ 9 kg) participated in the balance and walking rehabilitation training as shown in Fig. 6. The experiments were approved with IRB No. SIAT-IRB-200715-H0512.

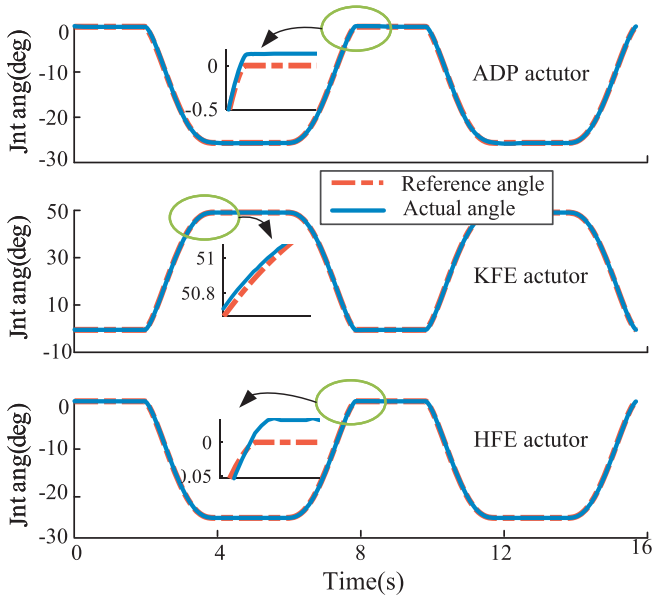


Fig. 7. Time series for the joint angle of the right leg during the squatting exercise. Both the actual and reference angles are shown in the figure.

TABLE II
CONTROLLER PARAMETERS IN EXPERIMENTS

| Controller parameters | Value |
|---|---|
| CoM height $Z_{CoM}$ | 0.883m |
| Controller gains $K_{\vartheta[i]x}$ | [-3.7, 13.5, 6.8] |
| Controller gains $K_{\vartheta[i]y}$ | [-3.0, 12.2, 6.0] |

## B. Balance Rehabilitation Training

The balance rehabilitation training involved squatting and tilting training. The squatting training required the vertical movement of the human body's CoM. In the tilting rehabilitation training, the subjects were instructed to wear the exoskeletons and control their CoM in four directional movements: forward, backward, left, and right. Fig. 7 shows the reference and actual joint angles during the squatting training. The squatting training involved the rotations of the hip, knee, and ankle joints in the sagittal plane, which resulted in the changes in the angles of the ADP, KFE, and HFE actuators. Only the right leg joint angles were recorded due to the symmetrical movements of the legs. The maximum absolute errors between the reference and actual angles were 0.20°, 0.29°, and 0.14° for the ADP, KFE, and HFE actuators, respectively. The mean absolute errors were 0.077°, 0.079°, and 0.043°, respectively, for each actuator. The standard deviations of the errors were 0.10°, 0.12°, and 0.06°, respectively. The ranges of motion for the ADP, KFE, and HFE actuators during the squatting training were between −27.23° and 0°, 0° and 51.43°, and −24.42° and 0°, respectively. The range of motion in each exoskeleton joint falls within the range of motion for the human joints (Table II), thereby making the exoskeleton-assisted rehabilitation training feasible for patients.

Fig. 8 shows the reference and actual angles of each left leg joint during the tilting rehabilitation training are shown in the Fig. 8. The HEE actuator did not undergo a rotation in the tilting rehabilitation training, resulting in the angle of the HEE actuator to remain as 0. The maximum absolute errors for the reference and actual angles were 0.11°, 0.23°, 0.11°, 0.19°, and 0.07° for the AIE, ADP, KFE, HFE, and HAA actuators, respectively. The root mean square tracking errors (RMSE) were 0.045°, 0.074°, 0.055°, 0.033°, and 0.027°, respectively. The range of motion for the AIE, ADP, KFE, HFE, and HAA actuators were between −8.86° and 9.08°, −33.09° and 0° degree, 0° and 54.06°, −24.41° and 0°, and −8.86° and 9.08°, respectively. All angles fell within the range of motion of the human joints.

The ZMP trajectory was measured by the F/T sensors and represented in Fig. 9. Fig. 9a depicts the ZMP position at different moments. Fig. 9c shows the ZMP trajectory in the horizontal plane. The range of the ZMP motion in the x and y axes was from −0.37 to 8.44 cm and from −13.25 to 12.81 cm. The support surface of the exoskeleton ranged from −12.6 to 16.4 cm on the x axis and −25.65 to 25.65 cm on the y axis. The minimum distance of the ZMP from the support surface boundary was 7.94 and 12.4 cm on the x and y axes, respectively. The maximal absolute errors on the x and y axes were 1.2 and 1.8 cm, respectively. The mean absolute errors were 0.38 and 0.64 cm, respectively. At the beginning of the tilting training, the ZMP moved 4 cm toward the positive x axis, direction due to the CoM shift during squatting.

## C. Self-Balancing Walking Rehabilitation Training

Fig. 10a and 10b depict the reference and actual ZMPs in the x and y axes, respectively. Each step had 12 cm length (Fig. 10a). The actual ZMP of different participants in both axes can converge to the reference values under the feedback control algorithm as shown in Fig. 10a and Fig. 10b, indicating that AutoLEE-II can maintain balance when used by different people. The mean absolute errors on the x and y axes were 2.19 cm and 3.73 cm, respectively. The maximum absolute value of error in the x axes direction occurs at 134.4 seconds during the walking of the second subject, with a maximum absolute error of 9.5 cm; the maximum absolute value of error in the y axes direction occurs at 12.7 seconds during the walking of the second subject, with a maximum absolute error of 11.6 cm. The tracking error between the actual and reference ZMPs was especially prominent during the transition from single support to double support because the elastic mechanical deformation of the exoskeleton during this process caused the exoskeleton's foot to prematurely touch the ground, which can cause a significant impact force between the ground and the foot and result in the ZMP tracking error. The minimum distance of the ZMP from the support surface boundary was 3.6 and 4.0 cm on the x and y axes, respectively. The range of motion for the AIE, ADP, KFE, HFE, and HAA actuators were between −10.04° and 10.02°, −28.32° and 0°, −54.06° and 0°, −25.27° and 0°, and −9.75° and 9.16°, respectively. All angles fell within the range of motion of the human joints.

## D. Muscle Activity

AutoLEE-II was designed to assist patients who cannot rely on active muscle contraction to complete their rehabilitation

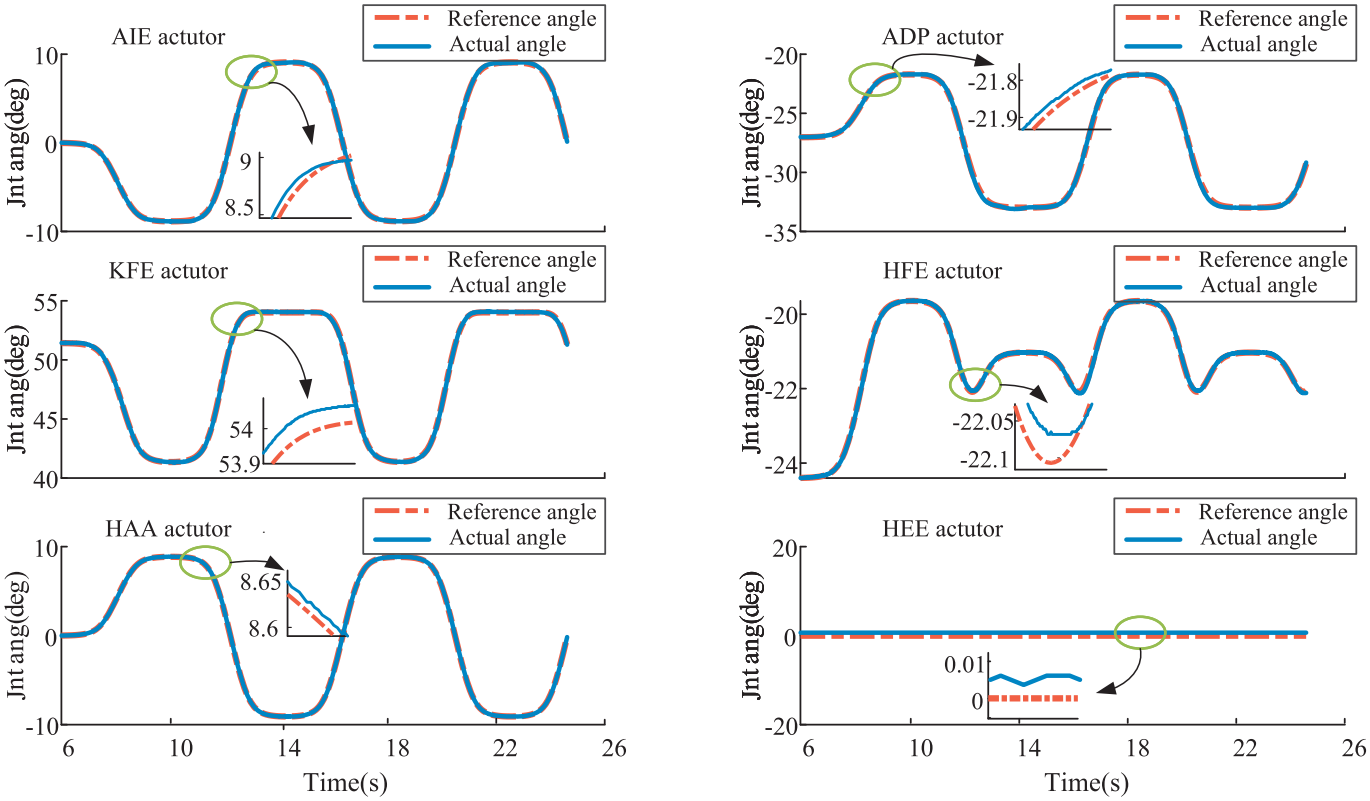


Fig. 8. Reference and real trajectories for the joint angle during the tilting exercise. The part with the maximum error in each figure is intentionally enlarged and displayed.

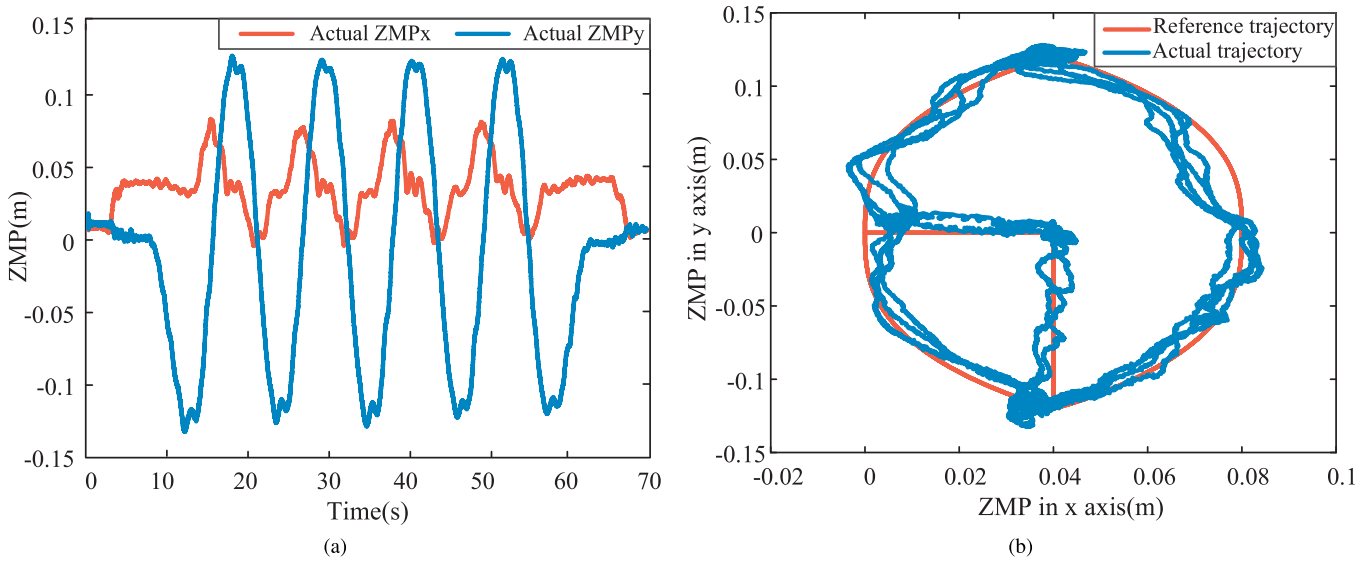


Fig. 9. Reference and real trajectories for the joint angle during the tilting exercise.: (a) ZMP position at different moments; and (b) ZMP trajectory in the horizontal plane.

training. Therefore, the muscle activity of these patients during the exoskeleton-assisted rehabilitation training should be lower than that of those independently completing their rehabilitation training. Five males participated in the rehabilitation training experiment under both "with and without exoskeleton" conditions to validate the exoskeleton's functional performance. The EMG signals from the participants' lower limb muscles were collected during the experiment to calculate their muscle activities. The recorded muscles include the vastus lateralis, rectus femoris, semitendinosus, gastrocnemius, soleus and biceps femoris muscles. These are the primary muscle groups in the lower limbs that generate force during the rehabilitation training. Figure 11 depicts the test scheme and the position of the EMG electrodes. The EMG signals of the lower limb muscles of each subject were recorded using the Biometrics PS850 system (Biometrics, Britain). The EMG data were sampled

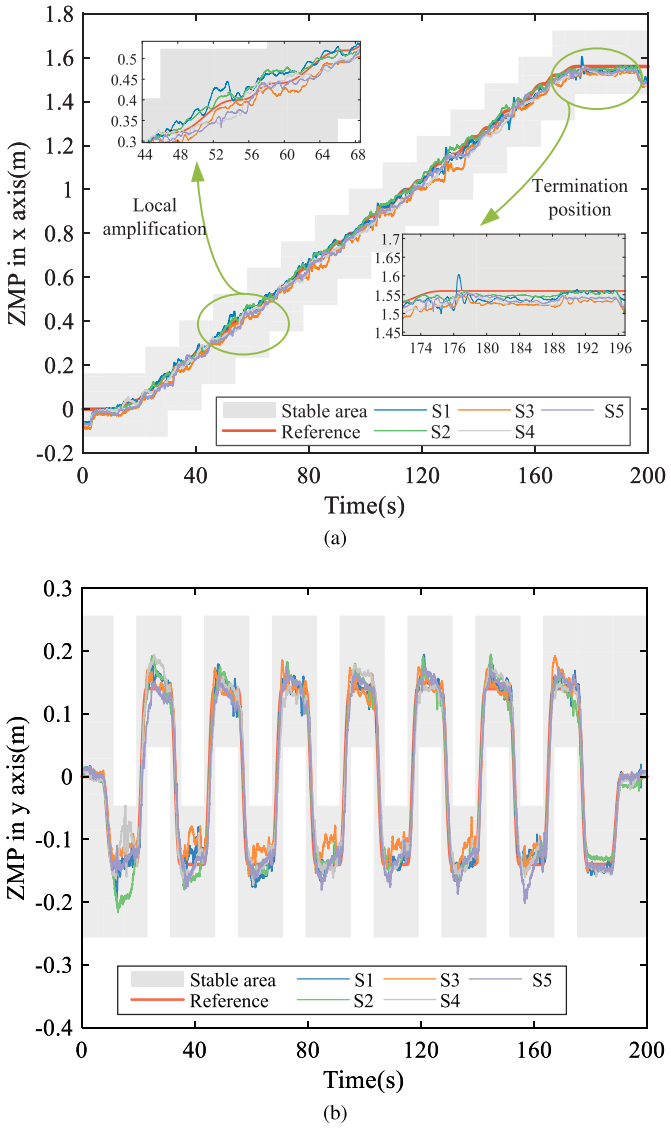


Fig. 10. ZMP movement during the gait training. The red line depicts the reference position. The blue line shows the real position. The gray region represents the support surface range. (a) Movement in the sagittal axis direction. (b) Movement in the coronal axis direction.

at 1000 Hz frequency. The raw EMG signals were band-pass filtered (20–450 Hz) in the electromyography system, rectified, and low-pass filtered (fourth-order Butterworth, 6 Hz cut-off frequency) in MATLAB (MathWorks). The muscle activity was presented as a percentage of the maximum voluntary isometric contraction (% MVIC). Accordingly, 100% MVIC of the muscles was measured according to [33]. The EMG data collected during the exercise were normalized to their muscles' respective MVIC trials and expressed as % MVIC. The average of the normalized data of the eight muscles was used as the evaluation index for the muscle activity of the lower limb during the exercise and expressed as % MVIC.

The final results were reported in the form of the mean ± standard error of the mean (SEM) as shown in Table III. The muscle activities of the subjects' low limbs while performing the three movements of squatting, tilting, and walking without exoskeleton were 47.17±3.64%MVIC, 42.94±5.28%MVIC, and 58.55±4.42%MVIC, respectively, while those of the

TABLE III
RANGE OF MOTION OF EACH JOINT OF THE HUMAN LOWER LIMB

| Joint | DOF | Range of motion |
|---|---|---|
| Hip | adduction/abduction (HAA) | −30° +60° |
| | flexion/extension (HFE) | −125° +25° |
| | endo/exorotation (HEE) | −30° +60° |
| Knee | flexion/extension (KFE) | 0° +130° |
| Ankle | inversion/eversion (AIE) | −35° +15° |
| | dorsi/plantarflexion (ADP) | −50° +30° |

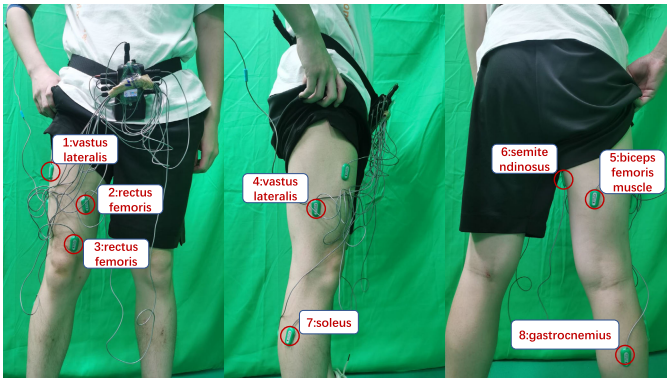


Fig. 11. Test scheme and position of the EMG electrodes.

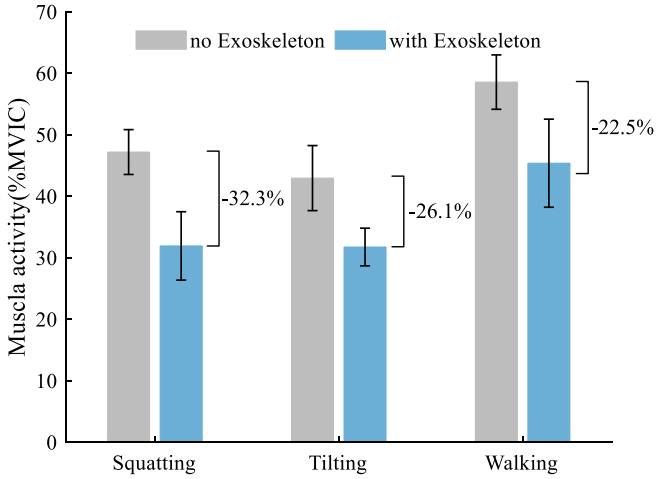


Fig. 12. Muscle activities of the lower limb under different lateral walking conditions.

subjects' low limbs under the assistance of an exoskeleton were 31.91±5.56%MVIC, 31.73±3.06%MVIC, and 45.36±7.16%MVIC, respectively. Compared to the case without an exoskeleton, muscle activity reductions were observed during squatting (32.3%), tilting (26.1%), and walking (22.5%).

## V. DISCUSSION

The exoskeleton-assisted rehabilitation training has immense potential in aiding the recovery of patients with SCI and improving their quality of life. The ability to perform multiple rehabilitation movements in the self-balance mode plays a vital role in improving the efficiency of the exoskeleton-assisted rehabilitation [34]. This work presented a self-balancing exoskeleton designed to aid in the rehabilitation training of individuals with SCI. We designed

TABLE IV
MUSCLE ACTIVITIES OF THE LOWER LIMBS UNDER DIFFERENT CONDITIONS

| Subject | Squatting | | Tilting | | Walking | |
|---|---|---|---|---|---|---|
| | no exo | with exo | no exo | with exo | no exo | with exo |
| S1 | 51.6414 | 21.7747 | 60.7085 | 23.0517 | 49.7870 | 40.0170 |
| S2 | 34.3557 | 34.3627 | 41.0933 | 39.2954 | 72.4491 | 45.4069 |
| S3 | 52.6728 | 50.8327 | 37.2834 | 27.8399 | 59.7432 | 22.9131 |
| S4 | 43.7555 | 19.6282 | 46.6356 | 37.9435 | 62.4503 | 51.9029 |
| S5 | 53.4705 | 32.9562 | 28.9875 | 30.5508 | 48.3349 | 66.5834 |
| mean | 47.1792 | 31.9110 | 42.9417 | 31.7363 | 58.5529 | 45.3647 |
| Â±SEM | 3.6458 | 5.5621 | 5.2889 | 3.0633 | 4.4213 | 7.1612 |

the exoskeleton with a biomimetic structure to ensure that it provides appropriate assistance to the patient's joints and avoid the discomfort caused by the axial deviation during the rehabilitation training. We also raised the CoM of the exoskeleton. In addition, a physical parameter-independent controller based on the CoM modification was designed to enable AutoLEE-II to maintain balance during walking. This controller can adapt to patients with different physical parameters. In the balance rehabilitation training experiment, the range of motion of each exoskeleton joint fell within the range of motion of the human joints. The human body ZMP moved up to 8.2 and 13.1 cm on the x and y axes, respectively. Meanwhile, in the walking rehabilitation training experiment, the minimum distance of the ZMP from the support surface boundary was 4.5 and 3.3 cm on the x and y axes, respectively. The ZMP consistently remained within the support surface boundary, reflecting the exoskeleton walking stability. The experiments proved that wearing the exoskeleton can reduce the lower limb muscle activity by approximately 20–30% when performing the same rehabilitation exercises.

### A. Performance Improvement

Compared to physical therapy done by a rehabilitation therapist and the non-self-balancing exoskeleton-assisted rehabilitation training, the self-balancing exoskeleton-assisted rehabilitation training is safer and more effective [35] because patients with an impaired balance can participate in their rehabilitation training while standing with the assistance of the self-balancing exoskeleton. The self-balancing exoskeleton's ability to maintain balance extends the range of the patient's CoM movement during the balance rehabilitation training. Nick Birch et al. examined the feasibility and the effectiveness of utilizing self-balancing exoskeletons to assist patients in rehabilitation training. Their results showed that the utilization of self-balancing exoskeletons for ambulation and exercise is feasible and safe for individuals with SCI [6].

There are currently four self-balancing exoskeletons available worldwide: REX, Atalante, AutoLEE-II and a self-balancing exoskeleton developed by University of Science and Technology of China [11], [12], [36] Compared to REX, AutoLEE-II has more DOFs for performing various actions, including turning, which REX cannot achieve. Unlike the control strategy of REX, that of AutoLEE-II incorporates compliant elements that results in the reduction of the impact force between the exoskeleton and the ground and improves the exoskeleton's balance capability. Compared to Atalante, the biomimetic structure of AutoLEE-II eliminates the axial deviation and improves user comfort during the operation [13]. The control strategy of AutoLEE-II can also adapt to patients with different physical parameters. AutoLEE-II can adapt to subjects with weights at least ranging from 50-73kg. The human-in-the-loop cooperative controller designed by Li [36] can only adapt to weight around 65-75kg. Thus, AutoLEE-II is robust to various wearers with different physical parameters.

### B. Limitations and Future Work

Although various self-balancing rehabilitation movements assisted by self-balancing exoskeletons have been achieved, this work still has limitations. AutoLEE-II lacks the capability to generate personalized gait based on the patient's specific physical parameters and needs, including height, weight and walking habits. In the future work, we will focus on designing personalized gaits, accounting for individual patients' body parameters, recovery stages, and walking habits while ensuring the exoskeleton's capability for self-balanced walking. Rehabilitation training experiments involving patients will also be conducted.

## VI. CONCLUSION

This work presents a self-balancing exoskeleton designed to aid SCI patients in their rehabilitation training and designs a biomimetic structure and physical parameter-independent controller. The stability of the control strategy is evaluated. The influence of the exoskeleton on the muscle activity of the subjects during rehabilitation training is also verified. The experiment validated the exoskeleton's ability to maintain balance during rehabilitation training and the feasibility of using the exoskeleton to assist patients in rehabilitation training. The experiments proved that wearing the exoskeleton can reduce the lower limb muscle activity by approximately 20–30% when performing the same rehabilitation exercises.

## REFERENCES

[1] A. Richardson, A. Samaranayaka, M. Sullivan, and S. Derrett, "Secondary health conditions and disability among people with spinal cord injury: A prospective cohort study," *J. Spinal Cord Med.*, vol. 44, no. 1, pp. 19–28, Jan. 2021.

[2] L. Teeter et al., "Relationship of physical therapy inpatient rehabilitation interventions and patient characteristics to outcomes following spinal cord injury: The SCIRehab project," *J. Spinal Cord Med.*, vol. 35, no. 6, pp. 503–526, Nov. 2012.

[3] D. Zbogar, J. J. Eng, W. C. Miller, A. V. Krassioukov, and M. C. Verrier, "Movement repetitions in physical and occupational therapy during spinal cord injury rehabilitation," *Spinal Cord*, vol. 55, no. 2, pp. 172–179, Feb. 2017.

[4] I. J. W. van Nes, R. B. van Dijsseldonk, F. H. M. van Herpen, H. Rijken, A. C. H. Geurts, and N. L. W. Keijsers, "Improvement of quality of life after 2-month exoskeleton training in patients with chronic spinal cord injury," *J. Spinal Cord Med.*, vol. 4, no. 1, pp. 1–7, Apr. 2022.

[5] E. Høyer, A. Opheim, and V. Jørgensen, "Implementing the exoskeleton ekso GTTM for gait rehabilitation in a stroke unit – feasibility, functional benefits and patient experiences," *Disab. Rehabil., Assistive Technol.*, vol. 17, no. 4, pp. 473–479, May 2022.

[6] N. Birch et al., "Results of the first interim analysis of the RAPPER II trial in patients with spinal cord injury: Ambulation and functional exercise programs in the REX powered walking aid," *J. Neuroeng. Rehabil.*, vol. 14, no. 1, pp. 1–14, Dec. 2017.

[7] C. Tefertiller et al., "Initial outcomes from a multicenter study utilizing the indego powered exoskeleton in spinal cord injury," *Topics Spinal Cord Injury Rehabil.*, vol. 24, no. 1, pp. 78–85, Jan. 2018.

[8] S. A. Kolakowsky-Hayner, J. Crew, S. Moran, and A. Shah, "Safety and feasibility of using the EksoTM bionic exoskeleton to aid ambulation after spinal cord injury," *J. Spine*, vol. 4, no. 3, pp. 1–8, 2013.

[9] S. Wang et al., "Design and control of the MINDWALKER exoskeleton," *IEEE Trans. Neural Syst. Rehabil. Eng.*, vol. 23, no. 2, pp. 277–286, Mar. 2015.

[10] C. Meijneke et al., "Symbitron exoskeleton: Design, control, and evaluation of a modular exoskeleton for incomplete and complete spinal cord injured individuals," *IEEE Trans. Neural Syst. Rehabil. Eng.*, vol. 29, pp. 330–339, 2021.

[11] C. Woods, L. Callagher, and T. Jaffray, "Walk tall: The story of rex bionics," *J. Manage. Org.*, vol. 27, no. 2, pp. 239–252, Mar. 2021.

[12] T. Gurriet, M. Tucker, A. Duburcq, G. Boeris, and A. D. Ames, "Towards variable assistance for lower body exoskeletons," *IEEE Robot. Autom. Lett.*, vol. 5, no. 1, pp. 266–273, Jan. 2020.

[13] Y. He, N. Li, C. Wang, L.-Q. Xia, X. Yong, and X.-Y. Wu, "Development of a novel autonomous lower extremity exoskeleton robot for walking assistance," *Frontiers Inf. Technol. Electron. Eng.*, vol. 20, no. 3, pp. 318–329, Mar. 2019.

[14] H. Geyer and H. Herr, "A muscle-reflex model that encodes principles of legged mechanics produces human walking dynamics and muscle activities," *IEEE Trans. Neural Syst. Rehabil. Eng.*, vol. 18, no. 3, pp. 263–273, Jun. 2010.

[15] S. Song and H. Geyer, "A neural circuitry that emphasizes spinal feedback generates diverse behaviours of human locomotion," *J. Physiol.*, vol. 593, no. 16, pp. 3493–3511, Aug. 2015.

[16] F. Dzeladini et al., "Effects of a neuromuscular controller on a powered ankle exoskeleton during human walking," in *Proc. 6th IEEE Int. Conf. Biomed. Robot. Biomechatronics (BioRob)*, Jun. 2016, pp. 617–622.

[17] Z. Li et al., "Human-in-the-loop control of a wearable lower limb exoskeleton for stable dynamic walking," *IEEE/ASME Trans. Mechatronics*, vol. 26, no. 5, pp. 2700–2711, Oct. 2021.

[18] T. Gurriet, M. Tucker, C. Kann, G. Boeris, and A. D. Ames, "Stabilization of exoskeletons through active ankle compensation," 2019, *arXiv:1909.11848*.

[19] M. Brunet, M. Pétriaux, F. Di Meglio, and N. Petit, "Fast replanning of a lower-limb exoskeleton trajectories for rehabilitation," in *Proc. IEEE 61st Conf. Decis. Control (CDC)*, Dec. 2022, pp. 2039–2046.

[20] K. H. Ha, S. A. Murray, and M. Goldfarb, "An approach for the cooperative control of FES with a powered exoskeleton during level walking for persons with paraplegia," *IEEE Trans. Neural Syst. Rehabil. Eng.*, vol. 24, no. 4, pp. 455–466, Apr. 2016.

[21] J. Liu, Y. He, J. Yang, W. Cao, and X. Wu, "Design and analysis of a novel 12-DOF self-balancing lower extremity exoskeleton for walking assistance," *Mech. Mach. Theory*, vol. 167, Jan. 2022, Art. no. 104519. [Online]. Available: https://linkinghub.elsevier.com/retrieve/pii/S0094114X21002718

[22] J. Li, D. Tian, J. Sun, M. Yin, Z. Wang, and X. Wu, "Stable walking feedback control for a self-balanced lower limb exoskeleton for paraplegics," *Int. J. Humanoid Robot.*, vol. 1, no. 1, pp. 1–18, Jul. 2023.

[23] Z. Sun, Y. Tian, H. Li, and J. Wang, "A superlinear convergence feasible sequential quadratic programming algorithm for bipedal dynamic walking robot via discrete mechanics and optimal control," *Optim. Control Appl. Methods*, vol. 37, no. 6, pp. 1139–1161, Nov. 2016.

[24] J. Park and Y. Youm, "General ZMP preview control for bipedal walking," in *Proc. IEEE Int. Conf. Robot. Autom.*, Apr. 2007, pp. 2682–2687.

[25] S. Kajita et al., "Biped walking pattern generation by using preview control of zero-moment point," in *Proc. IEEE Int. Conf. Robot. Autom.*, vol. 2, Sep. 2003, pp. 1620–1626.

[26] S. Kajita, H. Hirukawa, K. Harada, and K. Yokoi, *Introduction to Humanoid Robotics*, vol. 101. Berlin, Germany: Springer, 2014.

[27] A. L. Behrman, M. G. Bowden, and P. M. Nair, "Neuroplasticity after spinal cord injury and training: An emerging paradigm shift in rehabilitation and walking recovery," *Phys. Therapy*, vol. 86, no. 10, pp. 1406–1425, Oct. 2006.

[28] F. B. Horak, "Postural orientation and equilibrium," *Handbook of Physiology*. NY, USA: Oxford Univ. Press, 1996.

[29] S. L. Fritz et al., "An intensive intervention for improving gait, balance, and mobility in individuals with chronic incomplete spinal cord injury: A pilot study of activity tolerance and benefits," *Arch. Phys. Med. Rehabil.*, vol. 92, no. 11, pp. 1776–1784, Nov. 2011.

[30] G. Juras, K. Słomka, A. Fredyk, G. Sobota, and B. Bacik, "Evaluation of the limits of stability (LOS) balance test," *J. Human Kinetics*, vol. 19, no. 2008, pp. 39–52, Jan. 2008.

[31] A. L. Betker, T. Szturm, Z. K. Moussavi, and C. Nett, "Video game–based exercises for balance rehabilitation: A single-subject design," *Arch. Phys. Med. Rehabil.*, vol. 87, no. 8, pp. 1141–1149, Aug. 2006. [Online]. Available: https://www.sciencedirect.com/science/article/pii/S000399930600356X

[32] N. T. Shepard, M. Smith-Wheelock, S. A. Telian, and A. Raj, "Vestibular and balance rehabilitation therapy," *Ann. Otol., Rhinol. Laryngol.*, vol. 102, no. 3, pp. 198–205, Mar. 1993, doi: 10.1177/000348949310200306.

[33] J. W. Youdas et al., "Electromyographic analysis of trunk and hip muscles during resisted lateral band walking," *Physiotherapy Theory Pract.*, vol. 29, no. 2, pp. 113–123, Feb. 2013.

[34] G. Zeilig, H. Weingarden, M. Zwecker, I. Dudkiewicz, A. Bloch, and A. Esquenazi, "Safety and tolerance of the ReWalk exoskeleton suit for ambulation by people with complete spinal cord injury: A pilot study," *J. Spinal Cord Med.*, vol. 35, no. 2, pp. 96–101, Mar. 2012.

[35] N. Birch, J. Graham, and T. Priestley, "RAPPER II—Robot-Assisted PhysiotheraPy exercises WITH REX-powered walking aid in patients with spinal cord injury," *Spine J.*, vol. 16, no. 4, p. S70, Apr. 2016.

[36] Z. Li, T. Zhang, P. Huang, and G. Li, "Human-in-the-loop cooperative control of a walking exoskeleton for following time-variable human intention," *IEEE Trans. Cybern.*, vol. 9, no. 1, pp. 1–13, Oct. 2022.